# Evaluation of sensitivity for detecting different failure modes of epoxy matrix composites doped with graphene nanoparticles

M. Sánchez, R. Moriche, S. G. Prolongo, A. Ruiz, A. Jiménez-Suárez, A. Ureña

Materials Science and Engineering Area, University Rey Juan Carlos, C/Tulipán s/n, Móstoles, 28933, Madrid, Spain

maria.sanchez@urjc.es

## ABSTRACT

In recent years, the interest in monitoring the damage of composite materials by measuring the variation of electrical resistance is increasing because deformations and cracks generated in the structure produce changes in the electrical conductivity of the material.

In this work, the structural integrity of glass fiber composite materials with epoxy matrix doped with graphene nanoparticles is evaluated under in plane tests (interlaminar shear tests and fracture propagation tests in mode I and II). The results demonstrated the ability of graphene nanoparticles to form conductive networks in the epoxy resin with auto-detection capability of deformation and damage. In the interlaminar shear tests, permanent changes in resistance were associated to strain and delamination produced

during the test. In the case of fracture tests in mode I and II, the electrical resistance increased as the crack grew. The use of multiple electrodes has also allowed locating the area of damage generation in the material. Finally, the electrical response of discontinuities generated out of plane of the laminate was analyzed by means of cuts through the material.

**KEYWORDS:** Graphene nanoplatelets, electrical properties, functional composites, damage sensing.

## 1. INTRODUCTION

At present, composite materials are being extensively used in various industries such as aviation, automobile, marine etc. Among composite materials, Glass Fibre Reinforced Polymer (GFRP) composites are particularly used in the aircraft industry and wind turbine and blades. These components are subjected to several loads during their service life, which induce various kinds of invisible damages to the composites. The damage and failure of the composite materials are difficult to predict, which considerably decreases their reliability. Therefore, the composite material needs to be monitored at every moment during its operation.

The Structural Health Monitoring (SHM) techniques predict, interpret and evaluate the composite materials for damage and failure under different loading [1]. Most of these techniques are based on fiber Bragg grating sensors [2,3] and guided Lamb waves [4,5]; however, they still have many limitations as they usually give only local information about damage and their signal interpretation is not easy.

The addition of carbon nanoparticles to polymer matrix allows the formation of an electrical network that gives the material a high piezoresistivity [6-9]. SHM based on the variation of electrical resistance has received much attention because conductive networks formed in the polymer are sensitive to deformation and damage, even at low loads.

Graphene nanoplatelets (GNPs) with a two-dimensional structure are composed of several layers of stacked graphite nanocrystals, which makes them ideal conductive reinforcements [10-12]. Besides, graphene-based materials have shown gauge factors among the highest ever reported [13]. The higher strain sensitivity of graphene composites may be induced by larger intercontact area among the graphene nanofillers due to their 2-D structure and that might make larger contact resistance change than 1-D structure carbon nanofillers. This involves that two-dimensional nanoflakes usually show a piezoresisitivity one order of magnitude higher than that of nanowires, since their electrical percolation network is largely susceptible to geometrical changes and discontinuities [14].

The addition of GNPs to glass fiber composite materials allows the detection and location of damage by measuring variations in the electrical resistance of the material, as it has been demonstrated in previous works [15-18]. In the present work, the incorporation of GNPs in a percentage above the percolation threshold increased the conductivity of glass fiber composite materials. The sensitivity of the material to delamination has been analyzed during interlaminar shear tests and propagation of fracture in mode I and II. The use of several electric contacts has also enabled the location of damage in the composite material. The electrical response of the material caused by out of plane damage has been also analyzed using several channels.

## 2. METHODOLOGY

### 2.1. Materials

The polymer used as matrix of the nanoreinforced materials was an aeronautical grade epoxy resin produced by *Huntsman*, with a formulation based on DGEBA (*Araldite LY556*) cured with an aromatic amine (*Araldite XB3473*). Graphene nanoparticles functionalized with amine groups (GNP-$NH_2$) were incorporated as nanoscale reinforcement. These GNPs have an average lateral size of 5 μm and a thickness of less than 4 nm and were supplied by *CheapTubes*. Unidirectional glass fiber fabric purchased from *Hexcel* with the denomination *HexForce® 01031 1000 TF970*, type E fabric UD 4H Satin, was used as traditional reinforcement. It was made of E-glass fibers (E-GF) with an unbalanced weight distribution of fibers in warp/weft directions (87/13). The thickness of the fabric was 0.24 mm and its nominal weight 305 g/$m^2$.

### 2.2. Multiscale composites manufacturing

Multiscale composite materials were fabricated using epoxy resin doped with 12 wt. % of GNP-$NH_2$ and a glass fibre volume fraction of 50 % by hand lay-up, in order to reduce filtration phenomena. The dispersion of GNPs was performed on the monomer using a two-stage process optimized in a previous work that combined the application of ultrasounds for 45 min followed by three cycles of calandering [19]. The combination of dispersion processes allowed to achieve that most of the GNPs were extended and did not present a wrinkled structure. Afterwards, the GNP/epoxy mixture was degassed removing the occluded air by applying vacuum at a temperature of 80 ° C for 15 min. Then, the hardener was added in a weight ratio of 100:23 (LY556 / XB3473).”

The composite material was manufactured by hand lay-up through the stacking of layers up to reach the final thickness of the samples. Both, nanoreinforced matrix and glass

fiber fabric layers, were pre-heated up to 80 °C. The fiberglass fabric was placed in an open mold, and the doped resin was poured over each glass fiber layer. To favor the impregnation of the fibers and to eliminate trapped air, a roller was manually passed. The curing of the laminate was then performed in a hot plates press (*Fontijne LabEcon300*) in two stages: (1) low pressure (30 kPa) up to reach the gel time (45 min) to favor the flow and infiltration of the doped resin into the dry fabric; (2) a second stage at higher pressure (600 kPa) to favor compaction until the end of the curing process.

### 2.3. Structural health monitoring tests

The interlaminar shear tests and fracture propagation tests in mode I and II were performed on a *Zwick/Roell Z100* test machine load cell of 5 kN. During the tests, the electrical resistance of the samples was measured at various points using a source meter *Agilent 34410A* and the electrical contacts were made with silver paint to decrease the contact resistance. All specimens were electrically isolated from the mechanical testing fixtures using an isolating adhesive tape. The crack growth in mode I and mode II was recorded.

The interlaminar shear tests were performed according to ASTM D2344, the electrical contacts were placed at the top and the bottom of the specimen and the electrical resistance was measured in four channels simultaneously defined by 1, 2, 3 and 4 (Figure 1a). The purpose of these tests, in addition to monitoring the deformation, is to locate the damage on the tested specimen.

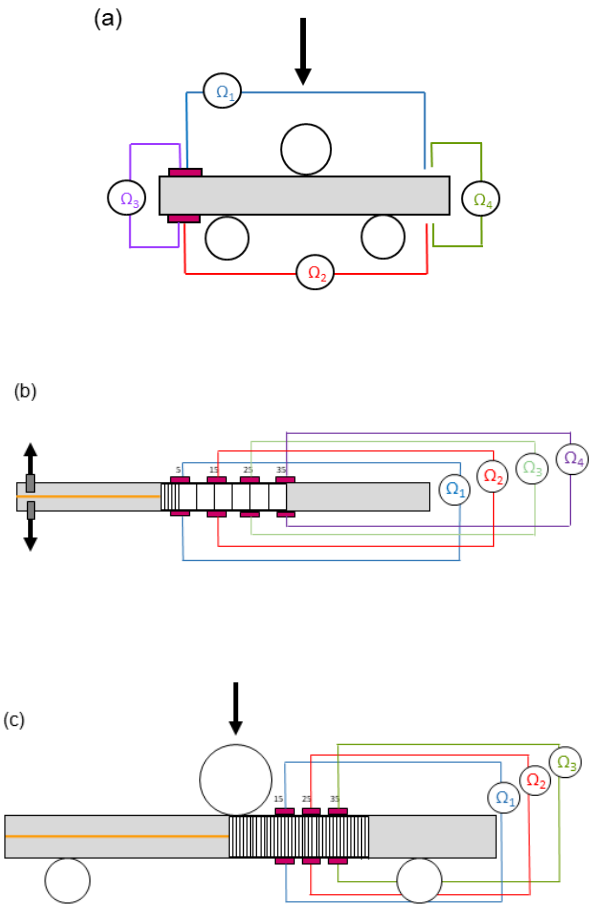


Figure 1. Schematic of the arrangement of the electrical contacts for the monitoring of multiscale composite materials in (a) interlaminar shear tests and (b and c) fracture propagation tests in mode I and mode II, respectively.

The characterization of the electrical behavior of the sensor during the growth of a delamination was also analyzed. For this purpose, fracture propagation tests in mode I and mode II were performed. The fracture propagation tests in mode I were made according to ASTM D5528 (Standard Test Method for Mode I Interlaminar Fracture Toughness of Unidirectional Fiber-Reinforced Polymer Matrix Composites). The

Double Cantilever Beam (DCB) specimens had dimensions of 125 × 25 × 3 mm. The teflon insert that defines the pre-crack was placed during the manufacturing of multi-scale material and had a length of 50 mm. The configuration of the measuring electrodes on the specimen consisted of eight electrodes placed at the top and the bottom of the sample to measure the electrical resistance across the thickness (Figure 1b). The contacts were located at 5, 15, 25 and 35 mm from the end of the insert. The goal of this test was to determine several factors such as the minimum distance of the crack to the contacts to detect delamination and its sensitivity to its progress.

After the propagation of the delamination in mode I, top and bottom surfaces remain separated avoiding electrical contact in those areas where the progress of delamination has taken place. However, when the delamination grows in mode II, the surfaces remain in contact and it could lead to a different electrical behavior. To analyze this phenomenon, tests following the AITM 1-0006 standard (Determination of interlaminar fracture toughness energy, Mode II) at a speed of 1 $mm \cdot min^{-1}$ were made. The dimensions of the specimens were 110 × 25 × 3 mm. The teflon insert had a length of 50 mm. In comparison to DCB test, the electrical contact line at a distance of 5 mm from the end of the insert was eliminated to avoid the application of load at the contact point during the test by the action of the top roller. The rest of the contacts were located at a distance of 15, 25 and 35 mm from the end of the insert (Figure 1c). The electrical resistance was measured again, through the thickness between two opposite points.

Apart from the tests based on standards, other tests were carried out producing cracks by means of cuts through the material with the purpose of characterizing the electrical response of discontinuities perpendicular to the plane of the laminate. The tests are described in the results section in order to facilitate their understanding.

To develop a strain and damage sensor, it is important to evaluate the relation between the applied load and the displacement on the sample and the piezoresistivity of the sensor. The normalized electrical resistance was calculated using the following equation (1):

$$R_N = \frac{R(t) - R_0}{R_0} \quad (1)$$

where $R$ ($t$) is the electrical resistance during the test and $R_0$ is the initial electrical resistance of the specimen.

## 3. RESULTS AND DISCUSSION

### 3.1. Monitoring of ILSS tests

Figure 2a shows the variation of the normalized resistance as a function of the strain, as well as the time domain curve of an ILSS representative test. Up to a beam depth of ~ 1.75 mm, the normalized electrical resistance underwent a gradual increase due to an increase of the distance between GNPs [20]. When damage occurred in the material, a drop in the stress of the mechanical curve is registered and an abrupt increase of the electrical resistance took place.

The damage that occurred in the specimen and broke the network of conductive paths created by the GNP in the multiscale matrix were not detectable until point (1) in Figure 2a. This would define the minimum size of detectable delamination or crack. Points (2) - (5) were associated with pronounced increases in the normalized electrical resistance. Each of the jumps corresponded to a drop of load in the mechanical curve,

therefore, corresponded to the appearance or propagation of delaminations and / or cracks in the matrix.

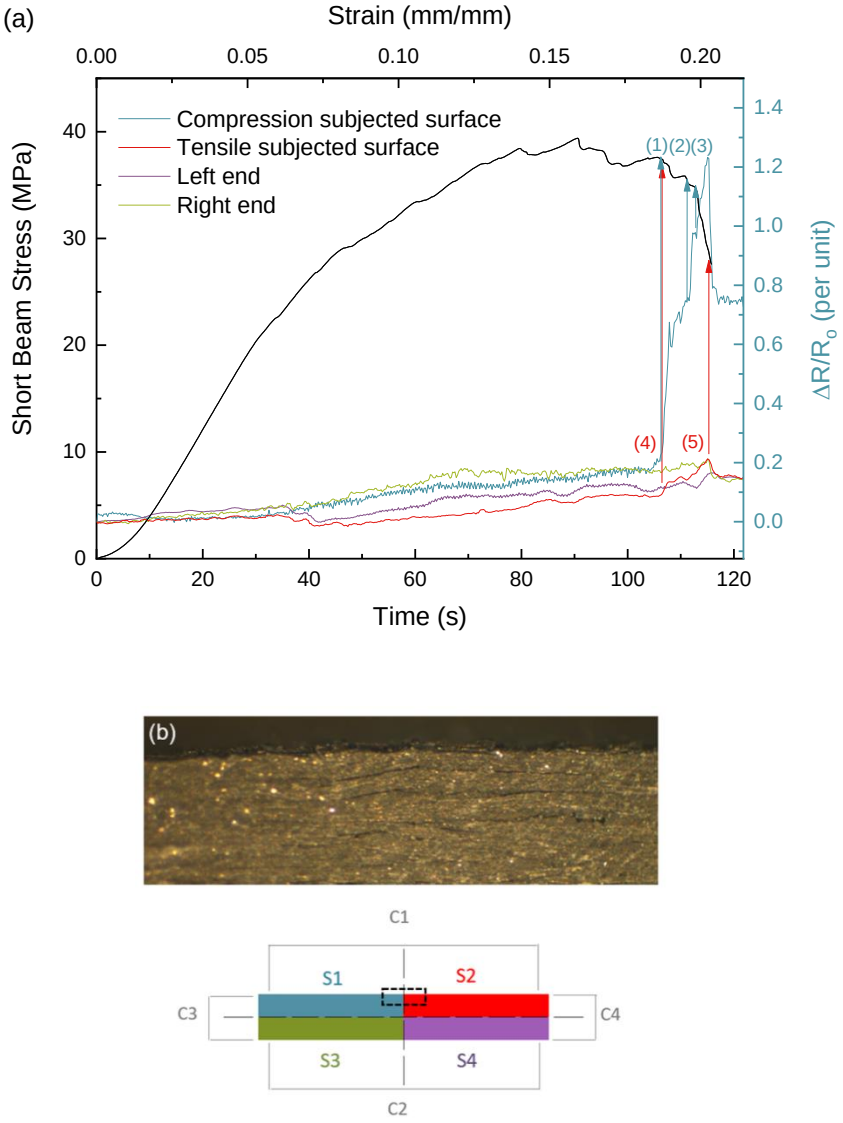


Figure 2. Monitoring of ILSS tests: (a) electrical response and mechanical curves of the test and (b) image of the damage located at the quadrants S1 and S2 (dashed line).

Variations in the slope of the electrical resistance were observed in the channels located on the surfaces subjected to compression and tensile loads, points (1) - (3) and (4) - (5), respectively. The increase of normalize electrical resistance at compression surface

between these points was around 100 % and in the case of tensile surface around 10 %. Böger et al. [21] obtained lower resistance changes, in the range of 20-40 % by the addition of carbon black into a system similar to the one studied, and between 10-15 % using CNT as reinforcement of epoxy matrix, recording the electrical signal at the edges of the specimen.

The increase of normalized electrical resistance on the compressed surface is approximately 10 times higher than the one registered on the tensile surface. For this reason, it can be concluded that discontinuities created in the material are located in the upper section of the specimen. The slight increase measured by the tensile channel is due to the damage located in a volume that overlaps with the measurement volume of this channel producing the observed augmentation. The gradual response recorded by the channels at the edges of the specimen allowed establishing that the failure took place at the central part of the sample. This information, together with the previous reasoning, located the damage at the upper central part of the specimen.

In order to confirm that the reasoning is correct, the tested sample was observed by an optical magnifying glass. Figure 2b shows that the damage was located at the region indicated above and, therefore, demonstrating the ability of the sensor to detect and locate the produced damage.

### 3.2. Monitoring of fracture propagation in mode I and II

Detection and monitoring of the growth of delaminations in composite materials is critical because in most cases they are internal and cannot be detected visually. For this reason, the electromechanical behavior of the multiscale composite materials was analyzed under mode I and mode II interlaminar fracture toughness tests.

### 3.2.1. Growth of delamination in mode I

The behavior of the sensor against the growth of delamination in mode I in one of the monitored tests is shown in Figure 3. The variation of the normalized electrical resistance and the force-displacement curve are represented together with the schematic of the channels placed at a distance of 5, 15, 25 and 35 mm from the end of the insert.

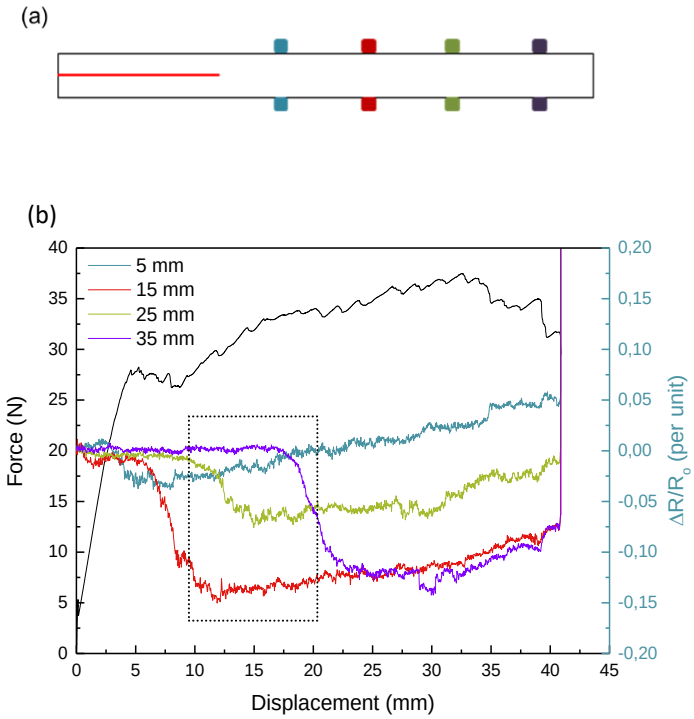


Figure 3. (a) Schematic of the test and (b) Force-Displacement and electrical response curves of mode I.

Three regions were distinguished in the monitored channels: in the first region, the normalized electrical resistance remained constant; in the second one, the electrical resistance diminished; and in the third region, a progressive increase of the electrical resistance was observed. Each zone can be related to three phenomena that occurred during the test. The stability in region I was related to delaminations that were not

detectable by the measuring channel because there was no appreciable change in the electrical resistance as it occurred out of the region that influences the measured electrical resistance, i.e. the delamination was formed at a distance greater than the maximum detectable by the sensor. In addition, the channels closest to the end of the insert were the first in detecting the onset of the delamination.

There was a point, for all channels, from which region II was defined, in which the normalized resistance began to decrease with a slope of $-8 \pm 2$ N·mm$^{-1}$. The decrease in electrical resistance was due to the compression state that appeared in the region between electrical contacts before the propagation of delamination. This phenomenon was previously observed in the analysis of the evolution of stresses during delamination onset and propagation by the finite element method model of the laminate structure [22,23]. The compression state favored the generation of conductive paths along the thickness of the specimen and produced the reduction of the electrical resistance.

Finally, the beginning of region III corresponded to a new change of trend, where the normalized electrical resistance increased with a slope of $(1.4 \pm 0.4) \cdot 10^{-4}$ mm$^{-1}$. Note that the increase of the electrical resistance is progressive and significant abrupt increases were not observed. Nevertheless, small abrupt increases can be detected in the electrical curve, which corresponds to small drops in the mechanical behavior, attributed to the unstable propagation of the delamination.

It is also important to mention that the existence of the compressive region II would allow anticipate the appearance of delaminations in mode I associated to a decrease in electrical resistance prior to propagation. This would allow the repair of the component before of failure, and thus ensuring its structural integrity.

In order to correlate the crack length with the increase of the normalize electrical resistance, already shown in Figure 3b, Figure 4 represents the electrical response as a function of the delamination growth for all channels in the region indicated in Figure 3b with a square (dash line), taking zero at the end of the insert to facilitate the discussion of the electrical behavior. In order to correlate Figure 3b and Figure 4, crack lengths of 1 mm and 25 mm in Figure 4 correspond to displacements of 8 mm and 20 mm in Figure 3, respectively. It can be observed that region II, in all the channels, starts when the end of the delamination tip is at a distance of ~ 15 mm from the electrical contact line and extended until the delamination was passed at ~ 5 mm from it, where the electrical resistance began to grow (region III). In that way, the delamination can be detected at a distance of ~ 15 mm without passing through the measuring channel due to the compression stress located at the tip, reinforcing the idea mentioned of predicting delamination growths.

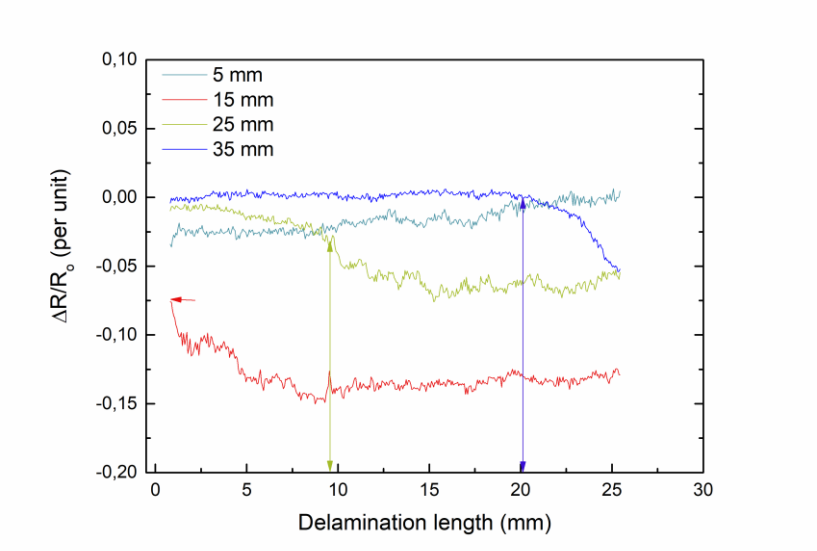


Figure 4. Electromechanical response depending on the progress of the delamination in mode I.

The results obtained by Zhang et al. [24] show a different trend since they do not obtain a response similar to that of region II described here. In this work, 2 wt. % of carbon black was used as reinforcement of an epoxy resin matrix in a multiscale material with glass fiber. The authors observed an exponential increase of the electrical resistance in the initial stage, which was followed by initiation and propagation of the delamination, giving rise to an electrical behavior similar to that explained for region III.

### 3.2.2. Growth of delamination in mode II

In order to analyze the electrical response in other fracture modes, tests monitoring the propagation of delamination in mode II were made. In this case, the surfaces remain in contact after delamination.

Figure 5 shows the normalized electrical resistance as a function of the delamination progress where two regions can be distinguished. The first region corresponded to non-existent electrical resistance change that was related to delaminations that were not detectable by the measuring channel. The second region started when the delamination was 4.7 ± 0.3 mm from the line defined by the electrical contacts. This point would define the beginning of an electrical behavior of the same characteristics as that recorded in region III of mode I, where the electrical resistance increased progressively with the progress of delamination.

The compression region that appeared in mode I was not observed in mode II, although Zhang et al. [24] registered this tendency and associated it to the strain of the material. This makes impossible to anticipate the damage until electrical resistance begins to increase.

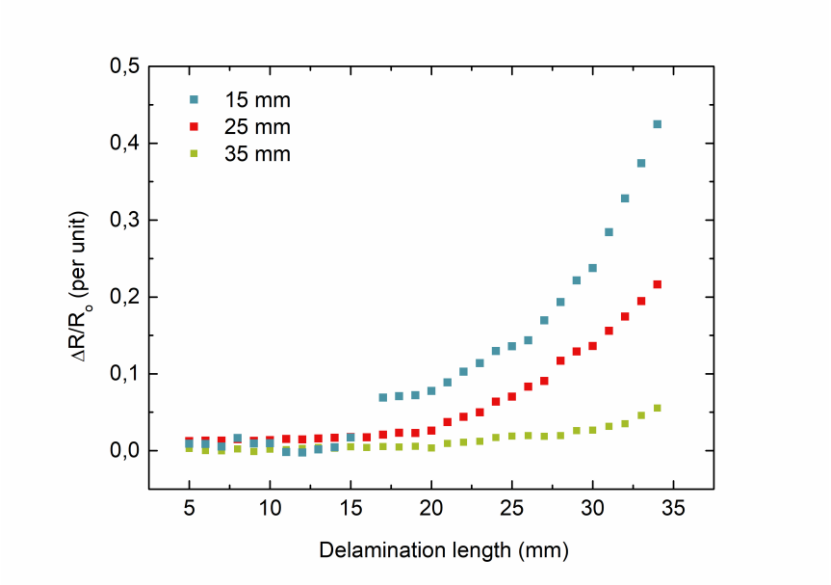


Figure 5. Electromechanical response as a function of the progress of the delamination in mode II.

It should be noted that the sensitivity in the second region of mode II is higher despite surfaces remain in contact. The sections in which the material is delaminated are displaced one with respect to the other and this phenomenon could be responsible for the increase in the sensibility.

### 3.2.3. Monitoring of damage out of the fiber plane

The electrical response of the material associated to discontinuities perpendicular to the plane of the laminate was also analyzed. Thus, a gradual cut was made through the thickness of the laminate and discrete measurements of the electrical resistance from one end of the laminate towards the interior were made. This allowed monitoring the influence of the progress of the damage by measuring different channels as it is seen in Figure 6.

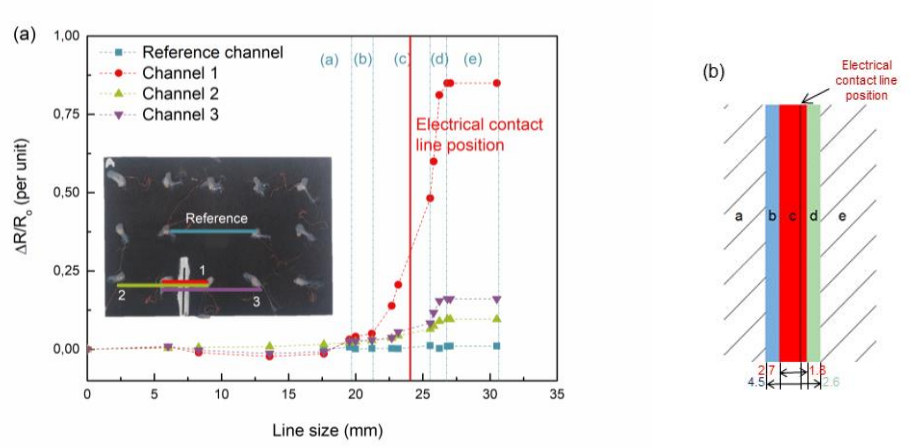


Figure 6. (a) Monitoring the cut line with a length of 35 mm and (b) scheme of the regions according to the electrical behavior.

Figure 6a shows the electrical response of the self-sensor due to the advance of a cutting line of 35 mm length. Four channels were monitored, the cutting line crossed three of them and the other one, far from the damage, was used as reference. Five regions were distinguished (a) - (e) according to the electrical behavior of the material caused by the generated damage. A scheme of the regions is represented in Figure 6b. In the region (a) the electrical resistance remained constant, so that the damage was not detectable by the sensor. This means that there was a minimum cutting line size, or maximum distance to the position of the contacts over which the damage was not detected through the measurement of the electrical resistance.

The cut was measurable when it was located at a distance of 4.5 mm from the monitored channels and this threshold defined the beginning of the region (b). The region (b) extended until the defect was located at a distance of 2.7 mm from the line joining the contact points that defined the measurement channels. In this region, the variation of the electrical resistance was minimal compared to that which occurs in the following regions.

The distance of 2.7 mm defined the beginning of the region (c), where the electrical response of the sensor showed a linear trend with a slope of $1.2 \cdot 10^{-1}$, $9.7 \cdot 10^{-3}$ and $1.4 \cdot 10^{-2}$ $m^{-1}$ for channels 1, 2 and 3, respectively. The reference channel was placed at a distance of 30 mm from the rest of the channels and that is why it did not detect the defect, since it is at a distance greater than the maximum distance detection. The slope, in all channels, remains constant until exceeding the line of contacts, included in the graph, at a distance of 1.8 mm.

From the results obtained, it can be deduced that the sensitivity of the channel 1 is two orders of magnitude higher than those of channels 2 and 3. This is due to the distance between contact points of channel 1 is half that in channels 2 and 3. Therefore, depending on the damage that is required to locate and how critical is its detection, the network of contacts will be designed for each component. The next region (d) corresponds to the zone of maximum sensitivity of the sensor, where the slope increased to $4.8 \cdot 10^{-1}$, $3.7 \cdot 10^{-2}$ and $1.4 \cdot 10^{-1}$ $mm^{-1}$ in the channels 1, 2 and 3, respectively. This region comprised the range of 1.8 to 2.6 mm, taking the position of the contacts as zero. The conclusion is that the sensitivity of the sensor increased considerably when the cutting line crossed the line of electrical contacts. With an appropriate design, this phenomenon could be used for the detection of critical crack size in structural components and the sensor will allow the acceptance or rejection of the structural integrity of a component.

Finally, the saturation of the electrical signal occurred (region (e)). This implied that the sensor is not sensitive to an increase of the damage length further than 2.6 mm from the contact line.

The results obtained in this work allow concluding that it would be possible to obtain a damage map of components designing the configuration of electrical contacts for the

evaluation of the integrity of this type of material, as it is possible using electrical impedance tomography [25]. This would allow detection, localization and quantification of the damage without the need to perform non-destructive tests that are usually done when the device is out of service. Viets et al. [26] implement this technology in multi-scale composite materials using CNT as nanoreinforcement of the matrix to create the electrical network that allows the monitoring of the damage.

## 4. CONCLUSIONS

Damage detection and location in glass fiber composite materials with epoxy matrix doped with graphene nanoparticles were analyzed. Damage was detected by means of abrupt increases in electrical resistance induced by breakage of the electrically conductive paths created by the graphene nanoplatelets.

In the case of ILSS tests, the use of several measurement channels allowed to locate the failure in the laminate, due the higher increase of electrical resistance registered by the electrical contacts closest to the failure. In the case of fracture propagation in mode I, damage was detectable from a distance to the contacts line of ~ 15 mm and ~ 5 mm when the fracture propagated in mode II. This fact established a greater detection to delaminations in mode I versus mode II.

This method also works for damage out of the plane of laminate. The use of low distance between electrical contacts gave rise to higher sensitive signals. The configuration design of electrical contacts would allow obtaining a map of the damage out of plane of components for evaluating the integrity of composite materials, taking into account the maximum distance of the damage from the position of the electrical contacts.

**Acknowledgements**

The authors would like to acknowledge the Ministerio de Economía y Competitividad of Spain Government (Project MAT2016-78825-C2-1-R) and Comunidad de Madrid Government (P2013/MIT-2862).

**References**

1. Giurgiutiu V. Structural health monitoring of aerospace composites. Academic Press, 2015.
2. Qirong Z, Cheng X, Guobiao Y. Experimental research on damage detecting in composite materials with FBG sensors under low frequency cycling. Int J Fatigue 2017;101:61-6.
3. Chen YC, Hsieh CC, Lin CC. Strain measurement for composite tubes using embedded, fiber Bragg grating sensor. Sens Actuators A 2011;167:63-9.
4. Yang B, Xuan FZ, Chen S, Zhou S, Xiao B. Damage localization and identification in WGF/epoxy composite laminates by using Lamb waves: Experiment and simulation. Compos Struct 2017;165:138-47.
5. Yelve NP, Mitra M, Mujumdar PM. Detection of delamination in composite laminates using Lamb wave based nonlinear method, Compos. Struct. 159 (2017) 257-66.
6. Vertuccio L, Guadagno L, Spinelli G, Lamberti P, Russo S. Piezoresistive properties of resin reinforced with carbon nanotubes for health-monitoring of aircraft primary structures. Compos Part B 2016;107:192-202.

7. Sanli A, Benchirouf A, Müller C, Kanoun O. Piezoresistive performance characterization of strain sensitive multi-walled carbon nanotube-epoxy nanocomposites. Sens Actuators A 2017;254:61-8.
8. Li C, Thostenson ET, Chou TW. Sensors and actuators based on carbon nanotubes and their composites: A review. Compos Sci Technol 2008;68:1227-49.
9. Xu H, Zeng Z, Wu Z, Zhou L, Liu M. Broadband dynamic responses of flexible carbon black/poly (vinylidene fluoride) nanocomposites: A sensitivity study. Compos Sci Technol 2017;149:246-53.
10. Ma J, Meng Q, Zaman I, Zhu S, Michelmore A, Kawashima N, Wang CH, Kuan HC. Development of polymer composites using modified, high structural integrity graphene platelets. Compos Sci Technol 2014;91:82-90.
11. Govorov A, Wentzel D, Miller S, Kanaan A, Sevostianov I. Electrical conductivity of epoxy-graphene and epoxy-carbon nanofibers composites subjected to compressive loading. Int J Eng Sci 2018;123:174-80.
12. Potts JR, Dreyer DR, Bielawski CW, Ruoff RS. Graphene-based polymer nanocomposites. Polymer 2011;52:5–25.
13. Li X, Zhang R, Yu W, Wang K, Wei J, Wu D, Cao A, Li Z, Cheng Y, Zheng Q, Ruoff RS, Zhu H. Stretchable and highly sensitive graphene-on-polymer strain sensors. Sci Rep 2012;2:870.
14. Kim YJ, Cha JY, Ham H, Huh H, So DS, Kang I. Preparation of piezoresistive nano smart hybrid material based on graphene. Curr Appl Phys 2011;11:S350eS352.
15. Moriche R, Jiménez-Suárez A, Sánchez M, Prolongo SG, Ureña A. Sensitivity, influence of the strain rate and reversibility of GNPs based multiscale composite materials for high sensitive strain sensors. Compos Sci Technol 2018;155:100-7.

16. Moriche R, Sánchez M, Jiménez-Suárez A, Prolongo SG, Ureña A. Electrically conductive functionalized-GNP/epoxy based composites: From nanocomposite to multiscale glass fibre composite material. Compos Part B 2016;98:49-55.
17. Mahmood H, Vanzetti L, Bersani M, Pegoretti A. Mechanical properties and strain monitoring of glass-epoxy composites with graphene-coated fibers. Compos Part A 2018;107:112-23.
18. Hao B, Ma Q, Yang S, Mäder E, Ma PC. Comparative study on monitoring structural damage in fiber-reinforced polymers using glass fibers with carbon nanotubes and graphene coating. Compos Sci Technol 2016;129:38-45.
19. Moriche R, Prolongo SG, Sánchez M, Jiménez-Suárez A, Sayagués MJ, Ureña A. Morphological changes on graphene nanoplatelets induced during dispersion into an epoxy resin by different methods. Compos Part B 2015;72:199–205.
20. Moriche R, Sánchez M, Jiménez-Suárez A, Prolongo SG, Ureña A. Strain monitoring mechanisms of sensors based on the addition of graphene nanoplatelets into an epoxy matrix. Compos Sci Technol 2016;123:65-70.
21. Böger L, Wichmann MHG, Meyer LO, Schulte K. Load and health monitoring in glass fibre reinforced composites with an electrically conductive nanocomposite epoxy matrix. Compos Sci Technol 2008;68:1886–94.
22. Turon A, Dávila CG, Camanho PP, Costa J. An engineering solution for mesh size effects in the simulation of delamination using cohesive zone models. Eng Fract Mech 2007;74:1665–82.
23. Pereira GF, Mikkelsen LP, McGugan M. Crack Detection in Fibre Reinforced Plastic Structures Using Embedded Fibre Bragg Grating Sensors: Theory, Model Development and Experimental Validation. PLoS ONE 2015;10(10):e0141495.

24. Zhang D, Ye L, Wang D, Tang Y, Mustapha S, Chen Y. Assessment of transverse impact damage in GF / EP laminates of conductive nanoparticles using electrical resistivity tomography. Compos Part A 2012;43:1587-98.
25. Loyola BR, La Saponara V, Loh KJ, Briggs TM, Bryan GO, Skinner JL. Spatial sensing using electrical impedance tomography. IEEE Sens 2013;132357–67.
26. Viets C, Kaysser S, Schulte K. Damage mapping of GFRP via electrical resistance measurements using nanocomposite epoxy matrix systems. Compos Part B 2014;65:80–8.